Surface & Coatings Technology 508 (2025) 132165

Contents lists available at ScienceDirect

Surface & Coatings Technology

journal homepage: www.elsevier.com/locate/surfcoat

Multi-layer structure improves wear and corrosion resistance of chromium

Xingwen Zhang [a], Qingzhong Mao [a,b,*], Zhifei Yu [a], Shaojia Shi [a], Zhan Liu [a], Yonghao Zhao [a,b,*]

[a] Nano and Heterogeneous Materials Center, School of Materials Science and Engineering, Nanjing University of Science and Technology, Nanjing 210094, China
[b] School of Materials Science and Engineering, Hohai University, Changzhou 213200, China

ARTICLE INFO

Keywords:
Multilayer chromium coating
Electrodeposition
Microstructure
Wear resistance
Corrosion resistance

ABSTRACT

Electrodeposited hard chromium coatings have been proven to significantly improve the friction and wear properties of matrix metallic materials. Due to the presence of microcracks, there is an inverse relationship between the friction and corrosion properties of hard chromium coatings. In this work, we designed and successfully prepared chromium coatings with alternating soft and hard chromium by pulse and direct current processes. The experimental results show that the multilayer structure can significantly reduce the microcrack density of the surface hard chromium coating. The wear rate and corrosion potential of the multi-layer Cr coating with five layers are 3.48×10^{-5}·mm^3·N^{-1}·m^{-1} and −524 mV, respectively. Compared with the single hard/soft chromium coating, the multilayer structure achieves a good synergy of wear resistance and corrosion performance. This is attributed to the multi-layer structure can effectively reduce the generation and propagation of microcracks. In the multi-layer structure, each layer can play a buffering role, reduce the brittleness of the overall coating, improve the wear resistance, and at the same time, in the multi-layer coating, more interfaces are formed, which prevent the further penetration of corrosive media to a certain extent.

1. Introduction

Wear and corrosion are the two main modes of equipment damage failure. Friction consumes one third of the world's primary energy, and the global economic cost of material wear is about 2 % of gross national product per year. Corrosion failure is even more serious, with the percentage increasing to 3–5 % [1–3]. Therefore, it is necessary to find a material or a solution that provides excellent wear and corrosion resistance under a wide range of operating conditions. Artificial chromium (Cr) protective coating has been proved to be effective in improving the service life and reliability of metal parts because of its excellent wear resistance and isolation from corrosion media [4–6]. Therefore, various Cr protective coatings are used in automotive manufacturing, marine engineering, aerospace and military equipment [7–9]. Compared with magnetron sputtering [10], chemical vapor deposition [11] and other physical methods, electrodeposition technology [12–14] has the advantages of convenient operation, low production cost and good coating uniformity, so it is the most widely used.

The structure and properties of Cr layer prepared by electrodeposition are mainly affected by current density and deposition temperature. Although high electrodeposition temperature can increase the deposition rate of the coating, it may introduce defects such as roughness and porosity of the coating [15]. If the temperature is too low, the deposition rate may be slowed down and the coating is not uniform. Although a smoother and uniform coating can be obtained with lower current density, the deposition rate is lower, while the higher current density can accelerate the deposition rate, but more internal stress and cracks may be introduced [16,17]. Electrodeposited Cr coatings are usually divided into hard Cr and crack-free Cr according to the hardness and microstructure of the coating. Hard Cr has high hardness, neat finish and excellent wear resistance, but hard Cr will form part of HCr, HCr in the process of electrodeposition, which leads to tensile stress in Cr matrix, which leads to high hardness and dense crack network [18–20]. The over-dense crack network not only significantly reduces the wear resistance of the coating, but also provides a suitable way for the corrosive agent to penetrate into the interface between the substrate and the Cr layer [21,22]. Pulse electrodeposition can reduce the hydride content and obtain crack-free Cr coating, which is conducive to improving the corrosion resistance of the Cr coating. However, the soft chrome coating has a lower hardness than hard chrome coating, and its wear resistance is poor [23–25]. In order to improve the wear resistance and corrosion resistance of Cr coating, a lot of work has been done. Celik

* Corresponding authors at: Nano and Heterogeneous Materials Center, School of Materials Science and Engineering, Nanjing University of Science and Technology, Nanjing 210094, China.
E-mail addresses: 216116000150@njust.edu.cn (Q. Mao), yhzhao@njust.edu.cn (Y. Zhao).

https://doi.org/10.1016/j.surfcoat.2025.132165
Received 11 March 2025; Received in revised form 13 April 2025; Accepted 14 April 2025
Available online 15 April 2025

and Benli [26] prepared tungsten carbide (WC-12Co) and chromium carbide nickel chromium (CRC NiCr) coatings on the surface of st37 steel by HVOF method, and systematically evaluated the comprehensive properties of the coatings. Shayan et al. [27] formed a layer of CrN on the surface of Cr coating by plasma nitriding to close the cracks of Cr coating and greatly improve the hardness and corrosion resistance of Cr coating. Imaz et al. [28] prepared Cr coating by direct current and pulse current method, and compared the corrosion resistance of Cr coating. Compared with direct current coating, crack-free PC coating has better corrosion resistance. DeMello et al. [29] shot peened the Cr coating to improve its surface morphology and wear resistance. However, the direction of this work is to adjust the structure of a single coating, and does not fundamentally solve the related problems. Ali et al. [30] prepared a 13–36 μm thick Cr-V-C coating by thermal diffusion at 900–1100 °C. After 500 thermal cycles and friction wear tests at 25–750 °C, its thermal fatigue and wear resistance were significantly better than untreated ductile iron. The performance improvement mainly comes from the dissolution of surface graphite during the TRD process, reducing the risk of graphite matrix interface failure.

Layered heterostructures formed alternately by components with different properties often show excellent mechanical and physical properties. Wu et al. [31] prepared a gapless atomic steel composed of a nanocrystalline layer and a coarse-grained core layer, discovering that the material exhibited enhanced strengthening effects. This enhancement is attributed to the gradient deformation behavior and mutual constraint effects between the gradient nanocrystalline layer and the coarse-grained layer. In layered materials, due to the non-uniform deformation and mutual constraints between soft and hard components, there is a multiaxial stress state in the components, which will further promote the storage of dislocations, which is conducive to better strength-plastic matching.

Therefore, we try to use electrodeposition method to realize the multi-layer structure alternately stacked by hard Cr and crack-free soft Cr, so as to block the continuity of cracks in the hard Cr layer and improve the wear resistance and corrosion resistance of the Cr coating. In this work, the microstructure, hardness, wear resistance and corrosion resistance of hard Cr coating, soft Cr coating and multi-layer alternating Cr coating were compared in detail. By understanding the relationship among electrodeposition process parameters, coating characteristics and performance characteristics, the microstructure of four kinds of coatings were accurately characterized by transmission electron microscope (TEM) and scanning electron microscope (SEM). The mechanism of tissue strengthening was analyzed and discussed. This study aims to provide new research ideas and methods for improving the service life of substrates and optimizing chrome coating processes.

2. Experiment

2.1. Coating preparation

According to different electrodeposition processes, four different types of coatings, hard chromium (HC), crack-free soft chromium (SC), 5-layer alternating hard and soft (5L), and 9-layer alternating hard and soft (9L), were to prepare on a 30CrNiMoV2 substrate with the compositions shown in Table 1. The composition of the plating solution includes a CrO_3 content of 230 g/L, sulfuric acid content of 2.8 mL/L. The sample is encapsulated with acrylic inlay, the surface to be plated is exposed, and the surface is mechanically polished with silicon carbide sandpaper. Subsequently, the fresh surface was polished with a particle size of 3.5 μm, until the surface is smooth and bright. To remove any remaining impurities, the workpiece then needs to be immersed in a chemical degreasing solution (120 g/L NaOH, 15 g/L Na_2CO_3, and 10 g/L Na_2SiO_3) heated to 70 °C for 8 min [17]. Subsequently, the workpiece was immersed in a 15 vol% hydrochloric acid solution for acid cleaning and activation for 30 s. Following this, it was removed and rinsed with deionized water before being dried. To improve adhesion between the coating and workpiece surface, the current should be slowly increased to the target value of 0.25 A/dm^2, while maintaining a plating solution temperature of 55 °C [18]. During plating, the workpiece and a lead-tin alloy with 13 wt% tin are the cathode and anode, respectively. To ensure uniform flow of the plating solution, a stirrer was used to keep stirring. The specific electrodeposition process parameters are shown in Table 2. The thickness of HC coating and SC coating is 100 μm. 5 L coating and 9 L coating are composed of soft and hard components alternately, in which the thickness of each layer of 5 L coating is 20 μm, and that of 9 L coating is 11 μm.

2.2. Microstructure characterization of coating

The phase detection analysis of the coatings was carried out using a Bruker-AXS D8 Advance X-ray diffractometer (XRD) with a Cu target produced by the German company Bruker. The scan range, test voltage and scan speed are 20°-145°, 40 kV and 5°/min, respectively. The determination of the phase relies on the comparison of the obtained spectra with the standard PDF cards (#06-0694).

The surface and cross-sectional morphology of the coatings was observed by FEI Quant250F field emission environmental SEM. The phase distribution and chemical composition of the samples were semi-quantitatively analyzed by using X-Max energy dispersive spectrometer (EDS).

The microstructure of the coatings was characterized using a Tecnai G2 20 LaB6 transmission electron microscope (TEM; FEI, USA). The TEM samples were precisely cut from the designated locations of the Cr coatings by focused ion beam (FIB) techniques (Helios Nanolab 450F1, FEI).

2.3. Friction performance and corrosion resistance test

HMV-G21DT (Shimazdu, Japan) microhardness tester was used to test the dehydrogenated coating. Diamond pyramid indenter with the angle between the two opposite sides is 136° was used. The test load and the holding time were 2.94 N and 10 s, respectively. In order to ensure the reliability of the data, each sample was measured at least 20 times.

Tribological properties were tested on a UMT-TriboLab tribometer

Table 2
Electrodeposition parameters of coating.

	Duty cycle	On-time (ms)	Off-time (ms)	Number of layers	Thickness (μm)	Jα (A/dm^2)
HC	–	–	–	1	100	35
SC	80 %	600	150	1	100	40
5 L (hard)	–	–	–	5	20	35
5 L (soft)	80 %	600	150		20	37
9 L (hard)	–			9	11	35
9 L (soft)	80 %	600	150		11	37

Table 1
Chemical constituents of 30CrNiMoV2 (wt%).

Fe	Cr	C	Si	Mn	S	Ni	Cu	P	Mo	V
Bal.	1.1	0.26	0.17	0.3	≤0.01	2.8	≤0.25	≤0.015	0.4	0.006

(Bruler, USA). The test was carried out in air at a controlled relative humidity of 50 ± 5 % and a temperature of 25 °C. The friction mode was reciprocating sliding friction, and the coating was subjected to friction test by ball-plate contact friction. The friction condition is dry sliding friction, the reciprocating stroke is 1 mm, the sliding speed is 10 mm·s^{-1}, the sliding load is 10 N, the test period is 1 h. The friction pair is Φ 6 mm Al_2O_3 ball.

Electrochemical tests were performed on a VERASCAN electrochemical workstations (AMETEK, USA). A three-electrode system was employed where graphite electrode is counter electrode, saturated calomel electrode is reference electrode and the sample with Cr coating is working electrode. The corrosion solution is 3.5 wt% NaCl aqueous solution to simulate a marine environment, and the temperature is controlled at room temperature. Before each test, the sample was immersed in the electrolyte for 2 h to stabilize the open circuit. The polarization curve potential ranges from $-0.5\ V_{VS.OCP} \sim 0.5\ V_{VS.OCP}$ and the scanning speed is 1 mV/s. The selected voltage amplitude of electrochemical impedance spectroscopy is 10 mV and the frequency range is 100 kHz ~ 10 mHz.

3. Results

3.1. Microstructure of coating

Fig. 1 shows the microstructure images of the surface and cross-section of different Cr coatings. It can be seen that the surface morphology of the coating is significantly affected by different electrodeposition processes. Fig. 1a shows the surface morphology of the HC coating. The HC coating has a relatively flat microstructure, but its surface is covered with a dense network of cracks. During the electrodeposition to form HC coatings, firstly Cr hydride with HCP microstructure is formed and subsequently undergoes a phase transition to pure Cr with BCC microstructure. The volume difference between the two phases is the root cause of crack formation [32]. As shown in Fig. 1d, the SC coating exhibits high surface roughness. Microscopic analysis reveals that the surface is predominantly composed of polyhedral particles formed by the clustering of Cr deposits with varying sizes. In contrast, the HC coating displays a crack-free planar morphology yet demonstrates relatively higher surface roughness. The suppression of cracking in the Cr layer can be attributed to the pulse electrodeposition process: (1) Enhanced diffusion of Cr ions near the cathode facilitates uniform deposition; (2) Increased overpotential for the hydrogen evolution reaction reduces competitive H_2 formation; (3) Oxidation of hydrogen ions within the anodic potential range minimizes hydride incorporation into the deposited layer [24]. The surface morphology of 5 L and 9 L coating is shown in Fig. 1g and j, and its microstructure consists of multiple hemispheres. The number of cracks in the multilayer coating compared with HC coating has been significantly reduced, in addition to the main cracks in the coating there are some small cracks. Compared with HC coating, the number of cracks in multilayer coating is obviously reduced, and there are some small cracks besides main cracks in coating. The difference is that the number of cracks in 5 L coating is less than that in 9 L coating, but the width of cracks is higher than that in 9 L coating. It should be noted that the outermost surface of 5 L and 9 L coatings is a hard Cr structure, but the surface structure is close to SC. This is because HC coatings have excellent stackability and can accurately inherit the structure of the substrate on the coating surface, so the hemispherical structure in the multilayer coating is inherited from the rough surface of the SC coating.

The microstructure of the cross-sections of the four coatings are shown in the rightmost column of Fig. 1. Fig. 1b illustrates multiple cracks in the HC coating, oriented parallel to the direction of deposition. During the electrodeposition process of the Cr coating, some HCr is produced. As HCr decomposes into Cr and H_2 during subsequent growth, a volume reduction of 15 % occurs. This reduction induces internal tensile stress within the coating. When this stress reaches the substrate's

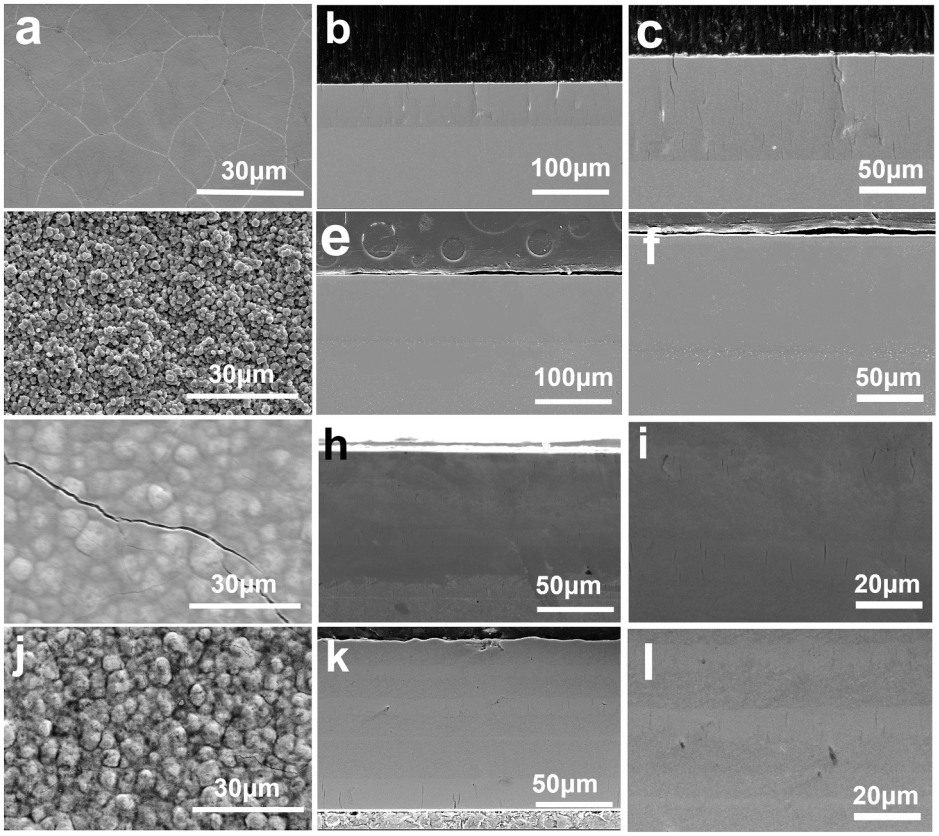

Fig. 1. Surface layer and cross-sectional structure of the coating: (a–c) HC coating; (d–f) SC coating; (g–i) 5L coating; (j–l) 9L coating.

release limit, cracks form. As the coating process continues, stress begins to accumulate once more, eventually leading to the formation of additional cracks. Compared to HC, there is no crack formation in the SC coating (Fig. 1e). The crack-free Cr layer in the 5 L layer and 9 L layer significantly blocks the crack propagation in the hard Cr layer. The grid method [32] was employed to determine the crack density on the coating surface, as shown in Fig. 2. The crack density of the HC coating was 634 pcs/mm^2, while the 5 L and 9 L coatings exhibited crack densities of 376 pcs/mm^2 and 418 pcs/mm^2, respectively. Additionally, surface roughness measurements were taken for all four coatings. The HC coating exhibited the smoothest surface, while the pulsed SC coating had the highest roughness value of 32.3 μm. The 5 L and 9 L coatings had roughness values of 13.8 μm and 21.3 μm, respectively.

Fig. 3 is the XRD pattern of four kinds of coatings. HC coating has only one strong diffraction peak in (222) crystal plane, indicating that there is a strong texture in (222) crystal plane in HC coating structure. Meanwhile, this diffraction peak has a large width, indicating that the grain size of hard Cr coating is also small. SC coating has diffraction peaks in many directions, and its intensity is similar to Cr standard card (PDF #06-0694), indicating that the grains in SC layer are anisotropic and there is no texture. 5L and 9L alternate coatings have diffraction peaks with different intensities in many directions, and the intensities are different, indicating that the grain orientation in the coating has certain non-orientation. Meanwhile, 5 L coating has a strong diffraction peak in (222) crystal plane, while 9 L coating has a low diffraction peak in (222) crystal plane. The values of average crystal size, dislocation density and micro strain effect are determined according to the X-ray analysis data using formula 1–3 [33]:

$$D = \frac{0.94\lambda}{\beta cos\theta} \tag{1}$$

$$\delta = \frac{1}{D^2} \tag{2}$$

$$\varepsilon = \frac{\beta}{4tan\theta} \tag{3}$$

where λ is the wavelength of the CuKa radiation (0.15406 nm), β represents the full width at half maximum (FWHM), and θ is the Bragg diffraction angle. The crystallographic parameters of the four coatings calculated based on the above formulas are shown in Table 3. Analysis shows that the grain sizes of different coating systems show significant differences: HC coating has the smallest grain size, SC coating has the largest grain size, while 5 L and 9 L coatings with multilayer structures have similar grain sizes. This phenomenon is closely related to the inhibition of grain boundary migration by multilayer structures. The dislocation density data further verified the distribution of grain size.

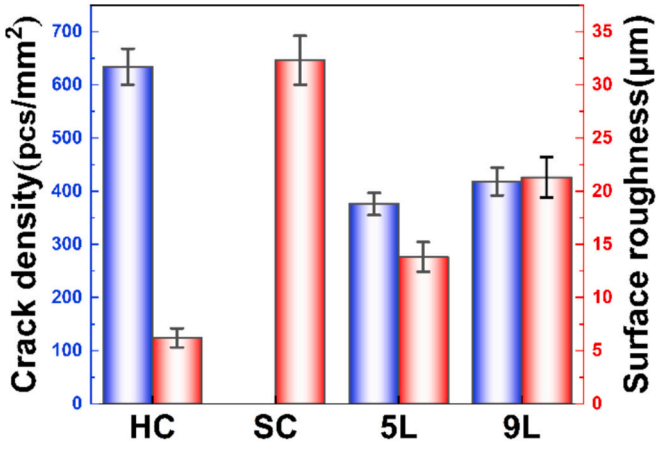

Fig. 2. Crack density and surface roughness of coatings.

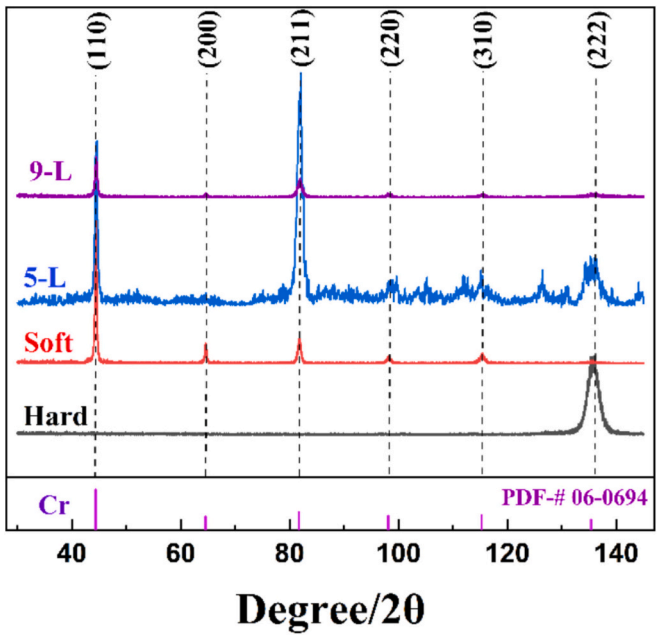

Fig. 3. X-ray diffraction patterns of four kinds of coatings.

Table 3
The XRD crystallographic information of four coatings.

	D (nm)	δ (10^{15} m^{-2})	ε
HC	42.3	4.6	0.26
SC	297.8	0.4	0.15
5 L	59.7	1.7	0.23
9 L	78.9	1.3	0.24

The HC coating showed the highest dislocation density (4.6 × 10^{15} m^{-2}), the SC coating showed the lowest dislocation density (0.4 × 10^{15} m^{-2}), and the 5 L (1.7 × 10^{15} m^{-2}) and 9 L (1.3 × 10^{15} m^{-2}) coatings were at the intermediate level, which was in line with the classic theory in the Hall-Petch relationship that grain refinement led to an increase in dislocation density. In terms of microstrain, HC (0.26 %), 5 L (0.23 %) and 9 L (0.24 %) coatings showed similar degrees of lattice distortion, while SC coating had the lowest microstrain value (0.18 %). This difference can be explained by the coating deposition mechanism: the high-energy deposition process of HC coating induces stronger residual stress accumulation, while the pulsed electrodeposition process of SC coating effectively releases lattice distortion. It is worth noting that the multilayer structure controls the microstrain within a reasonable range while maintaining a high dislocation density through the interface stress coordination mechanism.

The microstructures of the coatings were further analyzed using TEM, and Fig. 4 shows the bright field images of the TEM of the HC and SC coatings and their electron diffraction patterns. It can be seen from Fig. 4a that HC coating is mainly composed of columnar grains perpendicular to substrate direction, and there are a lot of defects between grains, which is consistent with the results in ref. [34]. Using the length of the columnar crystals in the short-axis direction as their grain size, the average grain size of the HC coating was measured to be about 53 nm. The microstructure of SC coating is composed of anisotropic equiaxed grains with an average grain size of 310 nm. In the local enlarged view of SC coating, we can see some dislocation clusters dispersed in the grains, which are defects formed during electrodeposition. The broadened diffraction spots also prove this phenomenon.

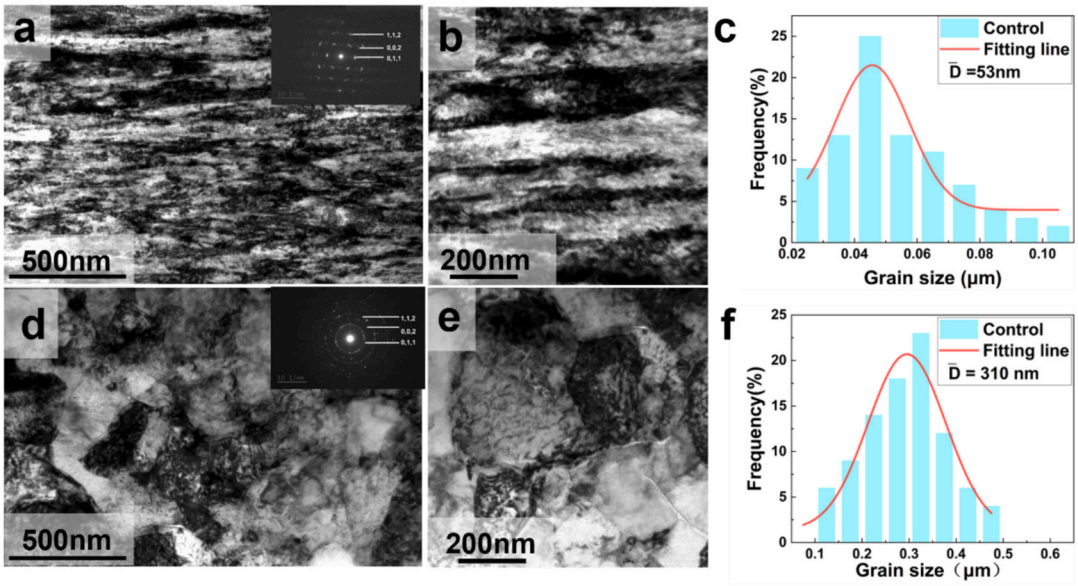

Fig. 4. Microstructure of coating (a) and (b) TEM BF images of HC coating; (c) grain size statistics of HC coating; (d) and (e) TEM BF images of SC coating; (f) grain size statistics of SC coating.

3.2. Performance of coating

Fig. 5 shows the hardness values of four types of coatings. The different electrodeposition processes have a significant influence on the hardness of the Cr coatings. The hardness of HC coating is as high as 805 HV, which is mainly due to the nanometer-sized grains and high density of defects as shown in Fig. 4. According to the Hall-Petch formula [35,36], the hardness of a metal is inversely proportional to the square root of the grain size, as well as the defects between grain boundaries, when dislocations move close to the grain boundaries, the grain boundary defects form an energy barrier that prevents the dislocations from continuing to move, thus increasing the strength and hardness of the material [37,38]. The hardness of SC coating is 619 HV, which is about 23.1 % lower than that of HC coating, mainly because the grain size of SC coating is 310 nm (Fig. 3), which is much higher than that of HC coating, according to Hall-Petch formula, the hardness of the material is closely related to the grain size and thus its hardness is lower, meanwhile, pulse plating is intermittent, which can control the plating layer effectively to reduce the generation of hydride, thus Reduces the generation of hydrogenated stresses and overall internal stresses in the plated layer, resulting in a decrease in the hardness of the plated layer.

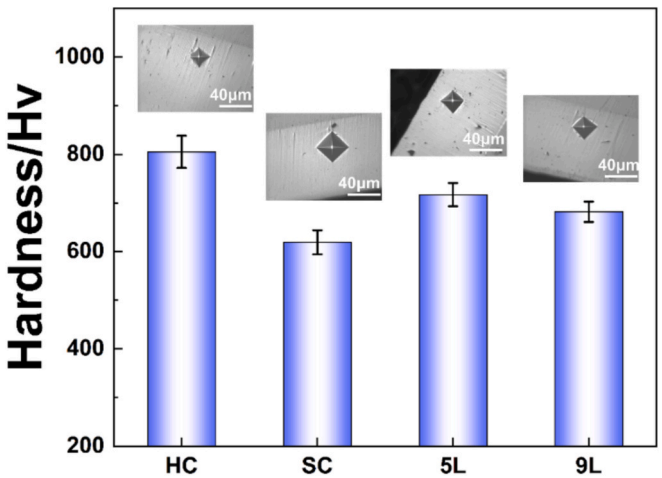

Fig. 5. Vickers hardness of four kinds of coatings.

The hardness of the 5 L and 9 L coatings is 717 HV and 682 HV respectively, which is between the hardness values of HC and SC. It should be noted that the outermost layer of the multilayer alternating plating is the HC coating, but the measured hardness is much different from that of the HC coating, due to the fact that it is difficult for the soft layer underneath to give support to the plated layer, which leads to a decrease in the hardness of the upper HC layer [39].

Fig. 6a shows the coefficient of friction (COF) curves of four types of coatings under a load of 10 N. The COF presents two stages as the friction progresses, namely the running-in stage and the stable stage. In the running-in stage, the friction coefficient is relatively high. This is because at the beginning of friction, the surface layer of the coating undergoes plastic deformation and surface oxidation. After entering the stable stage, although the friction coefficient tends to stabilize, there are still fluctuations present. The main reason for the unstable friction coefficient is the accumulation of friction debris (such as coating debris and oxides) at the interface between the friction pair and the coating, which will cause fluctuations in the friction coefficient. Meanwhile, the bonding mechanism of electrodeposited coatings mainly depends on physical adsorption or mechanical blockage, rather than diffusion bonding at the atomic level. During the friction process, there are local peeling and interface damage, leading to dynamic changes in the interface state [40,41]. Among the four types of coatings, the friction coefficient of the traditional HC coating is the highest at 0.64. In contrast, the friction coefficient of the SC coating is the lowest at 0.38. Compared to the HC coating, the friction coefficient of the SC coating has decreased by approximately 40.6 %. Additionally, the friction coefficients of the 5 L and 9 L coatings are also lower than that of the HC coating, at 0.51 and 0.58 respectively.

Wear volume is one of the important indicators of the wear resistance of coatings. A three-dimensional laser profilometer was used to reconstruct the wear tracks after fraction as shown in Fig.6b. Comparatively, it was found that under high-frequency friction with Al_2O_3 balls, the HC coating exhibits the deepest wear track, while the SC coating shows the shallowest wear track. The wear depth can be used to calculate the equivalent volume wear rate under different loads, specific formula as follows [42]:

$$K = \frac{A \cdot L}{F \cdot S} \tag{4}$$

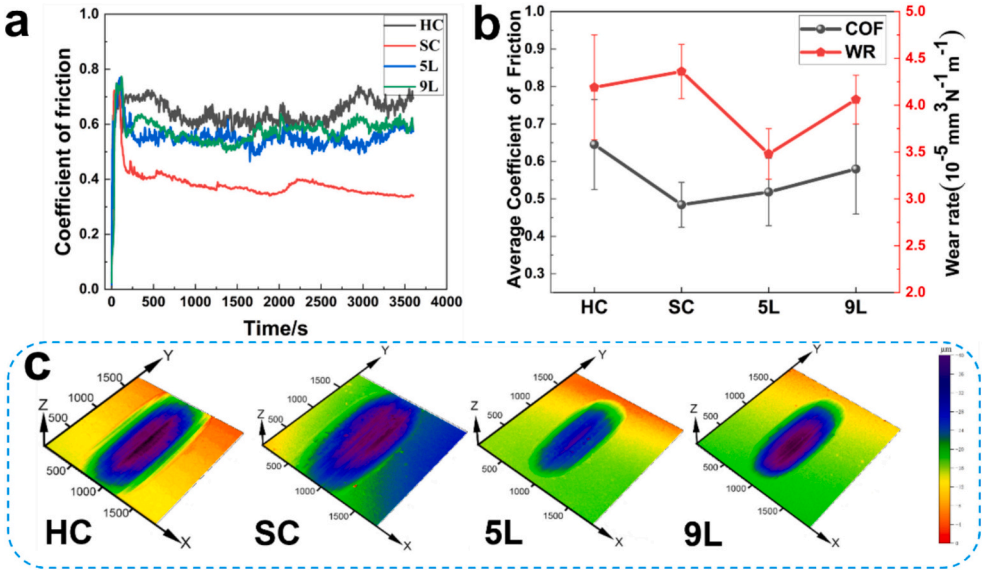

Fig. 6. Friction and wear properties of coating (a) friction curves of four kinds of coatings; (b) statistics of friction coefficient and wear rate of coatings; (c) three-dimensional diagram of wear marks of four kinds of coatings.

where *A* represents the cross-sectional area of the wear mark, obtainable from the wear mark's width and the radius of the Al_2O_3 sphere; *L* is the length of the abrasion mark; *F* is the applied load; S is the total travel of the friction process; commonly, *K* is measured in $mm^3 \cdot N^{-1} \cdot m^{-1}$. In terms of COF, the wear resistance of the SC coating and the multi-layer alternating coating is better than that of the HC coating. However, in terms of wear track depth, the performance of the HC coating and the multi-layer alternating coating is better than that of the SC coating. Fig. 6c shows the equivalent volumetric wear rates of the four coatings. When the load is 10 N, the wear rate of HC, SC, 5 L and 9 L is 4.19, 4.36, 3.48 and 4.06 ($10^{-5} \cdot mm^3 \cdot N^{-1} \cdot m^{-1}$) respectively. The wear rate of SC coating is the highest, the wear rate of HC and 9 L coating is similar, and the wear rate of 5 L coating is the lowest.

3.3. Microscopic morphology of wear track on coating

The tribological performance of the coatings is significantly correlated with their initial microstructural characteristics. As shown in Fig. 7, the analysis of wear morphology under the counteraction of Al_2O_3 balls using a scanning electron microscope indicates that different coating systems exhibit distinct failure mechanisms. The wear track width of the HC coating is 0.39 mm (Fig. 7a), with numerous grooves parallel to the sliding direction on the surface, accompanied by significant wear debris accumulation. High magnification observation (Fig. 7b) further reveals typical abrasive wear characteristics, manifested as shear microcracks perpendicular to the sliding direction, which are closely related to the stress accumulation effect under cyclic loading. Notably, the SC coating shows a wider wear track (0.61 mm), with the surface exhibiting not only parallel grooves but also a large amount of flaky spallation products (Fig. 7c). This layered spallation phenomenon originates from the brittle fracture mechanism caused by hardness mismatch at the contact interface-the softer SC surface layer undergoes lamellar separation under repeated shear, while the plastic deformation capability of the underlying 5 L coating effectively suppresses crack propagation. It is noteworthy that no microcracks were observed in the microstructure of the SC coating (Fig. 7d), confirming the stress-relieving effect of the pulsed electrodeposition process. The multilayer coating system exhibits a significant structural optimization effect: the wear track width of the 5 L coating is reduced to 0.56 mm (Fig. 7e), the density of grooves decreases by about 35 %, and flaky wear debris is significantly reduced. This improvement is attributed to the stress redistribution achieved by the interface sliding mechanism of the

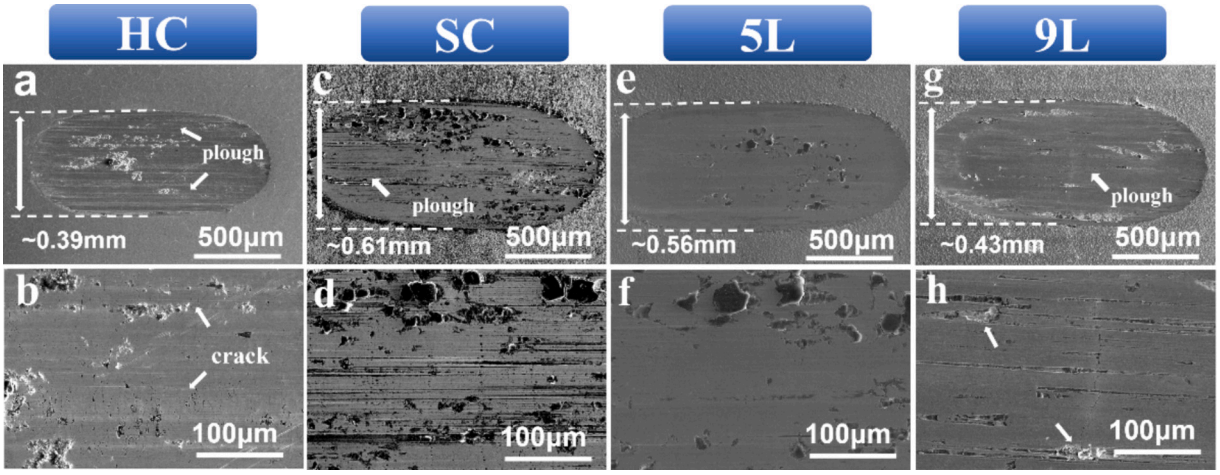

Fig. 7. Global (a, c, e, d) and local (b, d, f, h) morphology of wear tracks of four coatings.

hard/soft alternating layers. In contrast, the wear morphology of the 9 L coating shows abnormal deterioration (Fig. 7g), with increased groove width and depth, accompanied by micron-scale material spallation (Fig. 7h). This layer-dependent wear behavior may be related to the interface stress accumulation effect-excessive interlayer interfaces lead to local stress concentration, weakening the overall load-bearing capacity of the coating.

To further investigate the changes of various coatings undergo during wear, SEM-EDS element analysis was conducted on the furrows and wear debris within the wear tracks, as specifically depicted in Fig. 8. The surfaces of the wear tracks mainly consist of Cr and O elements, which indicates that all Cr coating wear tracks were covered with oxides. Inside the furrows of the wear tracks, fresh, unoxidized metal regions are exposed, while the deformed areas around the edges of the furrows have undergone some degree of oxidation. The grit size for the HC coating ranged from 2 to 10 μm, predominantly featuring irregular flake-like spallation. During the friction wear process, wear debris forms at the furrow edges through nucleation, expansion, interpenetration, and exfoliation. With further reciprocating friction, severe oxidation occurs [43,44]. At the same time, wear debris from the coating mixes with the opposing ball, further exacerbating wear. In contrast, the appearance of flake-like wear debris from the SC coating typically results from abrasive wear and spalling that occur during friction, which is a classic example of a lamellar wear mechanism. Throughout this process, the micromorphology of the material surface undergoes shear deformation due to external stress, leading to localized plastic flow. When the strain energy in these plastically flowing zones reaches a certain threshold, it causes the material to delaminate, forming flake-like wear products. However, the wear debris from the 5 L coating is significantly less in quantity compared to the other coatings, indicating that the 5 L coating possesses superior wear resistance.

3.4. Corrosion resistance of coating

3.4.1. Electrochemical performance of the coating

Fig. 9a illustrates the evolution of open circuit potential (OCP) over time for four types of coatings in a 3.5 wt% NaCl solution. The HC coating, characterized by a high density of defects, exhibits the most negative stable potential (−646 mV), indicating the highest thermodynamic tendency for corrosion. In contrast, the SC coating, with larger grain size and fewer internal defects, has a more positive potential (−447 mV) compared to the HC coating. The potentials of the 5 L (−461 mV) and 9 L (−496 mV) multilayer coatings fall between these two, suggesting that the alternating structure partially mitigates corrosion activity through an interfacial barrier effect; however, their protective performance remains inferior to that of the pure SC coating. Fig. 9b presents the dynamic potential polarization curves of four Cr coatings in a 3.5 wt% NaCl aqueous solution at 25 °C. Despite the distinct microstructures of the coatings, their polarization curves are similarly shaped, indicating that the variations in the multi-layered soft and hard structures do not significantly affect the corrosion behavior of Cr in the NaCl solution. Table 4 summarizes the corrosion potentials and current densities for each coating, determined using the Tafel extrapolation method. A more positive corrosion potential correlates with enhanced corrosion resistance, typically signifying a material's stronger redox capability, higher electron release capacity, and improved stability in corrosive environments. In electrochemical corrosion, metal experiences oxidation (anodic) and reduction (cathodic) reactions under an applied potential. The anodic reaction involves metal dissolution, while the cathodic reaction consumes electrons. The lower corrosion potential indicates the greater tendency of anodic reaction, which increases the possibility of metal dissolution and corrosion. Among the examined coatings, the HC coating exhibits the highest corrosion potential at approximately −658 mV, whereas the SC coating has the lowest at around −501 mV, representing a 23.8 % reduction in comparison to the HC coating. The corrosion potentials for the 5 L and 9 L coatings are −524 mV and −530 mV, respectively, indicating similar corrosion behaviors in the NaCl solution, with both outperforming the HC coating. Corrosion kinetics are reflected in the corrosion current density, which measures the metal corrosion rate per unit time. Table 3 shows that the HC coating has the highest corrosion current density at 1.83×10^{-6} A/cm^2, whereas the SC coating's current density significantly reduces to 2.53×10^{-7} A/cm^2. The multi-layer coatings present intermediate corrosion current densities of 6.65×10^{-7} A/cm^2 and 4.50×10^{-7} A/cm^2. Therefore, in the 3.5 wt% NaCl corrosion system, the SC coating exhibits superior corrosion resistance due to its crack-free nature, a characteristic greatly enhanced by the alternating soft/hard layered structure [18,28].

Polarization resistance is an important parameter that describes the metal material under electrochemical corrosion conditions, which reflects the resistance of the metal surface to electrochemical corrosion, the larger the polarization resistance, means that the metal has better corrosion resistance in the corrosive environment. Polarization resistance pertains to the impedance encountered by the electron or ion transmission through the electrochemical polarization layer formed on the material surface during electrochemical corrosion, when a specific voltage or current is applied. A higher polarization resistance equates to an increased resistance of the protective film formed on the material surface against corrosive penetration, thereby mitigating the rate of corrosion and enhancing the material's corrosion resistance. The polarization resistance (R_P) within the corrosion system is typically estimated via the Stern-Geary formula [45]:

$$R_P = \frac{\beta_a * \beta_c}{2.3 * I_{Corr} * (\beta_a + \beta_c)} \quad (5)$$

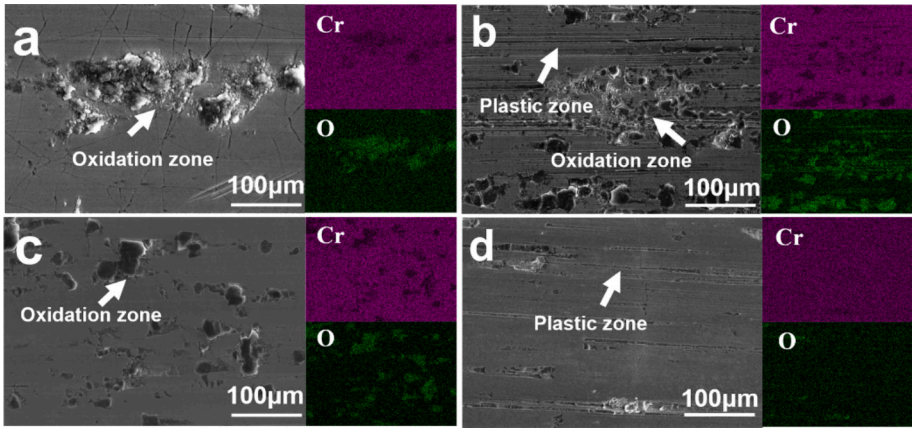

Fig. 8. EDS element distribution diagram of wear products of coating: (a) HC; (b) SC; (c) 5L; (d) 9L.

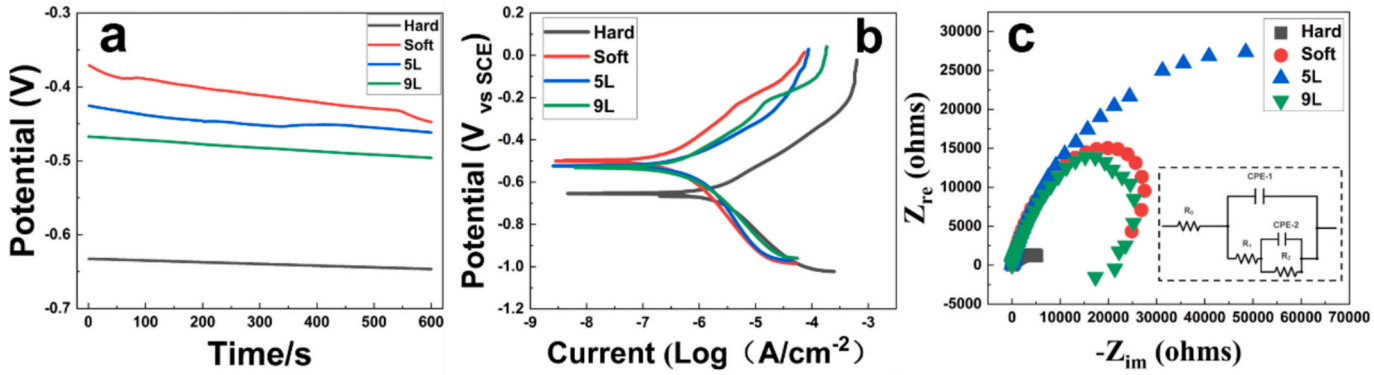

Fig. 9. Electrochemical performance of the coating: (a) open circuit voltage curve; (b) polarization curve; (c) electrochemical impedance spectroscopy, the inset is the equivalent circuit diagram.

Table 4
Electrochemical corrosion parameters of coating in 3.5wt%NaCl solution.

	E_{corr} mV_{SCE}	I_{corr} $mAcm^{-2}$	β_α mV	β_c mV	R_P Ωcm^2
HC	−658	$1.83{\cdot}10^{-6}$	4984	4877	$4.24{\cdot}10^{6}$
SC	−501	$7.53{\cdot}10^{-7}$	4022	3346	$5.70{\cdot}10^{8}$
5 L	−524	$6.65{\cdot}10^{-7}$	3296	5811	$1.38{\cdot}10^{9}$
9 L	−530	$4.50{\cdot}10^{-7}$	4843	5761	$2.54{\cdot}10^{9}$

where I_{Corr} signifies the corrosion current in the polarization curve; β_α and β_c denote the slopes of the anode region and the cathode region of the polarization curve respectively; and the fitting range lies 10 mV above and below the corrosion potential. Relevant values are presented in Table 3. It can be seen from the results that the polarization resistance of the coating is about the same as the corrosion current density, but the polarization resistance of the alternating coating is higher than that of the SC coating. It shows that this multi-layer structure makes the coating have better resistance to local corrosion, makes the material surface uniform corrosion, and delays the occurrence of corrosion damage.

Electrochemical impedance spectroscopy (EIS) is a crucial technique for assessing the corrosion resistance of materials. Fig. 9c presents the EIS data for four coatings in 3.5 wt% NaCl at room temperature under open-circuit conditions. The plot shows capacitive loops across mid to high-frequency ranges for the different coatings. The HC coating exhibits the smallest capacitive loop radius, while the 9 L coating shows the largest. As corrosion is fundamentally an electrochemical process, the size of the capacitive loop is indicative of the rate of electrochemical reactions. A larger loop radius corresponds to a slower reaction rate. The EIS experimental results indicate that the 5 L coating has the best corrosion resistance. Based on the comprehensive polarization and EIS curves, we found that multi-layer coatings exhibit superior corrosion resistance compared to single-layer coatings. Among them, the 9 L coating demonstrated the highest corrosion resistance, while the 5 L coating showed comparable performance. This enhancement is attributed to the optimized interfacial effects of the multi-layer structure. The structure comprises stacked layers of distinct materials, with each interface engineered to enhance cohesion and complementarity. Effective interface design reduces interfacial impedance, thereby minimizing interfacial reactions and charge transfer resistance, ultimately improving the overall electrochemical performance [46,47].

3.4.2. *Morphology of the coating after electrochemical testing*

Fig. 10 presents the surface morphology of four coatings following dynamic potential polarization curve testing. To ensure accuracy, the center of each test sample was selected as the primary observation point. Significant differences are observed in the corrosion patterns across the various Cr coatings. The surface of the HC coating (Fig. 10a and b) exhibits numerous corrosion scars. In electrochemical tests, surface defects are particularly susceptible to corrosion, leading to the formation of gas or solution products and causing surface bulging. Metal corrosion typically occurs unevenly due to variations in microstructure (e.g., grain boundaries, dislocations, and phase boundaries) and surface conditions (such as oxidation, adsorbed species, and stress distribution), resulting in differing local corrosion rates. In regions with rapid corrosion, material is preferentially consumed, forming depressions, while slower-corroding areas remain relatively intact, resulting in protrusions.

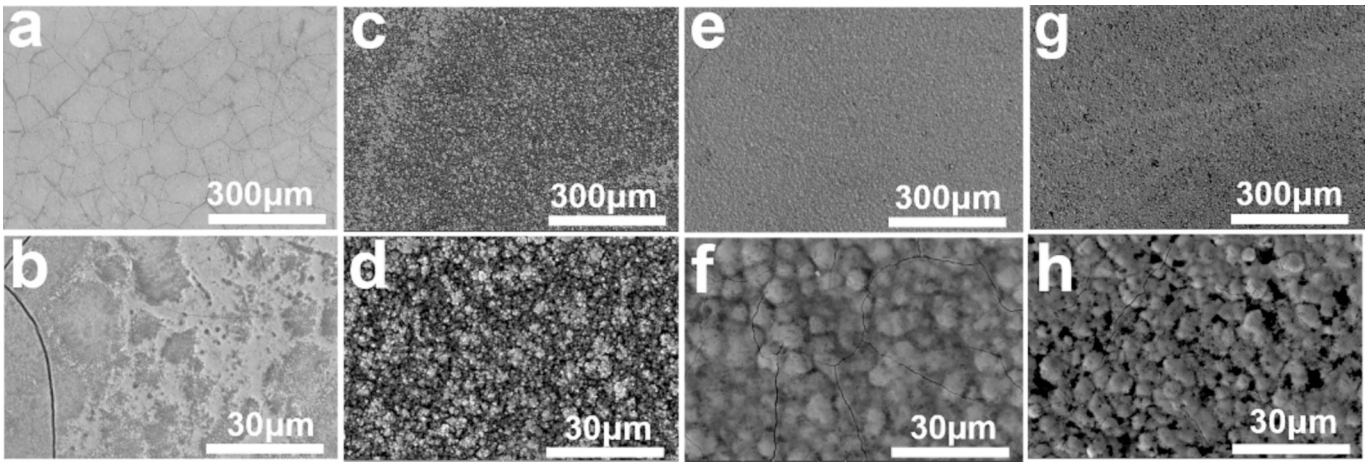

Fig. 10. Morphology of the coating after electrochemical test: (a) (b) HC coating; (c) (d) SC coating; (e) (f) 5L coating; (g) (h) 9L coating.

These raised structures can alter the surface properties, further influencing corrosion behavior and material applicability. In the SC coating, the corrosion severity is less pronounced than in the HC coating, as metal corrosion typically initiates at grain boundaries. Since the grain boundaries of the HC coating are nanocrystalline, it exhibits a higher tendency for corrosion. For the 5 L and 9 L coatings (Fig. 10e–h), no significant signs of local corrosion, such as pitting or intergranular corrosion, are observed. High-magnification images reveal only minor raised structures. The presence of physical or chemical barrier effects between the different layers of the multi-layered materials may inhibit the diffusion and infiltration of the corrosive medium. This barrier protection can slow the corrosion process and extend the material's service life.

4. Discussion

4.1. Effect of coating structure on wear resistance

The friction and wear tests show that the 5L alternating coating has excellent wear resistance. From the results of three-dimensional laser confocal scanning, it can be seen that the wear mark width and depth of multi-layer alternating coating are smaller than those of single HC coating and SC coating. According to the analysis of the friction behavior of the four coatings, as shown in Fig. 6, the highest COF of HC coating is 0.65 and the lowest COF of SC coating is 0.48. The morphology of wear marks of four kinds of coatings (Fig. 7) shows that the main friction form of HC coating is abrasive wear, while the main friction forms of SC coating and 9 L coating are abrasive wear and adhesive wear. The main form of wear for the 5 L coating is adhesive wear. By estimating the isovolumetric wear rate, it was found that the SC coating had the largest wear rate of 4.36×10^{-5}·mm^3·N^{-1}·m^{-1}, the HC coating had a wear rate of 4.19×10^{-5}· mm^3·N^{-1}·m^{-1}, and the wear rates of the multilayered coatings were smaller than both of them, with the 5 L coating having the lowest wear rate of 3.48×10^{-5}·mm^3·N^{-1}·m^{-1}.

Layered metal materials, which are alternately stacked by soft and hard components with significant differences in mechanical properties, generally have excellent comprehensive mechanical properties, such as high strength, good plasticity, strong work hardening ability and so on [48–50]. The excellent mechanical properties of this multi-layered material mainly come from the non-uniform plastic deformation between soft and hard components, resulting in plastic strain gradient, resulting in geometric necessary dislocation that coordinate plastic deformation [51,52]. These additional stored geometric necessary dislocation can lead to long-term back stress, resulting in additional strengthening and work hardening, which in turn increases the strength and plasticity of the material [53,54]. In a layered composite coating system, the gradient disparity in mechanical properties between the alternating soft and hard components induces a unique interface synergy effect. When subjected to external loads, the incompatible deformation between the hard phase (HC) with a high elastic modulus and the soft phase (SC) with a low elastic modulus generates a multiaxial stress field at the heterogeneous interface region. According to dislocation dynamics theory, this three-dimensional stress state facilitates the stacking and interaction of dislocations at the phase interface, significantly enhancing the material's work-hardening capability through dislocation proliferation and entanglement mechanisms. This strengthening mechanism, driven by heterogeneous interface control, allows the composite to maintain exceptional plastic reserves while retaining high strength, thereby achieving a synergistic improvement in both strength and plasticity. In contrast, a single-layer HC coating, despite its hardness of up to 860 HV, is prone to high internal stress and low fracture toughness. It is susceptible to the formation of a penetrating crack network under cyclic loading. This damage mode exacerbates abrasive wear by promoting three-body wear, leading to an increased volumetric wear rate. In contrast, the multilayer coating structure, which balances both hardness and toughness, not only exhibits high hardness and excellent wear resistance but also effectively mitigates crack propagation, enhancing overall wear resistance. The multilayer design compensates for the deficiencies in hardness or toughness inherent in single-layer coatings, offering superior wear performance under specific operational conditions.

4.2. Effect of multiple interfaces on corrosion resistance

The experimental results indicate that SC coatings and multilayer alternating coatings exhibit significantly better corrosion resistance than HC coatings. As shown in the TEM images, HC coatings are primarily composed of nanocolumnar crystals, while SC coatings consist of equiaxed crystals approximately 300 nm in size. Grain boundaries often harbor structural defects such as lattice imperfections and atomic misalignments. These defects can cause changes in interatomic distances and localized stress concentrations at the grain boundaries, making them more susceptible to attack by corrosive agents. Generally, because nanocrystals have a higher specific surface area and more grain boundaries, corrosive agents like Cl^- ions can more easily penetrate into the nanocrystal material, leading to rapid corrosion [55]. Moreover, due to their small grain sizes and high grain boundary energy, nanocrystalline materials may exhibit higher chemical reactivity, increasing their susceptibility to corrosion. In contrast, ultrafine-grained materials, having larger grain sizes than nanocrystals but still relatively small, usually possess fewer grain boundaries. This can make them more resistant to corrosion to some extent. The reduced number of grain boundaries in ultrafine-grained materials makes it harder for corrosive agents to penetrate, thereby slowing down the rate of corrosion.

The multi-layer Cr coating demonstrates exceptional corrosion resistance, which can be primarily attributed to its unique structural design and inherent microscopic characteristics. This advanced coating system consists of alternating layers of soft and hard Cr, with distinct and well-defined interfaces between each layer. The cumulative effect of these interfaces significantly enhances the material's resistance to corrosion, making it less susceptible to corrosive attacks [56]. When corrosion initiates, the behavior of a single hard Cr coating differs markedly from that of a multi-layer coating. In a single hard Cr coating, the corrosive medium can easily penetrate through the material via a dense network of micro-cracks, leading to rapid corrosion and potential severe damage. In contrast, the multi-layer coating, with its alternating soft and hard Cr layers, benefits from the interface between each soft Cr layer and the hard Cr layer, which acts as a barrier that impedes the further diffusion of the corrosive medium. As the corrosive medium penetrates one layer, it must overcome the interface between that layer and the next before continuing its progression. This layer-by-layer diffusion process complicates and hinders the path of the corrosive medium, effectively delaying the onset and progression of corrosion, and significantly enhancing the material's overall corrosion resistance [57]. Additionally, the combination of soft and hard phases not only increases the number of protective interfaces but also imparts a variety of protective properties. These properties work synergistically to resist the penetration of corrosive media, thereby further improving the material's resistance to corrosion.

5. Conclusion

In this work, we designed and prepared HC, SC and soft-hard multilayer Cr coatings by pulse and direct-current plating, and characterized and tested the microstructure, wear resistance and corrosion resistance of the four coatings. The main conclusions are as follows:

- The HC coating has a columnar structure with grains perpendicular to the substrate (approximately 53 nm), while the SC coating has equiaxed grains (approximately 310 nm).
- The crack density of HC coating reached 634 pcs/mm ^{2}, and the multi-layer coating (5 L: 376 pcs/mm ^{2}, 9 L: 418 pcs/mm ^{2})

significantly decreased. The alternating coating has a higher overall roughness than the pure HC coating due to the dense stacking of HC and the roughness of the SC substrate.

- Under a load of 10 N, the wear rate of the 5 L coating among the four coatings is the lowest, which is 3.48×10^{-5}·mm^3·N^{-1}·m^{-1}. The multi-layer coating combines the abrasive wear mechanism of HC and the adhesive wear mechanism of SC: the HC layer provides load support, while the SC layer disperses stress and suppresses crack propagation through plastic deformation, synergistically improving wear resistance.
- The corrosion currents of multi-layer coatings are all lower than those of single-layer coatings. Among them, the 9 L coating has the best corrosion resistance, with a value of 4.50×10^{-7} A/cm^2.
- The 5 L multilayer coating has the best wear resistance (wear rate of 3.48×10^{-5}·mm^3·N^{-1}·m^{-1}) and significantly improved corrosion resistance (corrosion current of 6.65×10^{-7} A/cm ^{2}) through the synergistic effect of HC and SC alternating structure, and its comprehensive performance is superior to that of single and 9 L coating, which is suitable for high load corrosion working conditions.

CRediT authorship contribution statement

Xingwen Zhang: Writing – original draft, Software, Methodology, Investigation, Data curation, Conceptualization. **Qingzhong Mao:** Writing – review & editing, Supervision, Funding acquisition, Conceptualization. **Zhifei Yu:** Methodology, Conceptualization. **Shaojia Shi:** Methodology, Conceptualization. **Zhan Liu:** Data curation, Conceptualization. **Yonghao Zhao:** Writing – review & editing, Validation, Funding acquisition, Conceptualization.

Declaration of competing interest

The authors declare that they have no known competing financial interests or personal relationships that could have appeared to influence the work reported in this paper.

Acknowledgments

Y.H. Zhao acknowledges financial supports from the National Key Research and Development Program of China (Grant No. 2021YFA1200203), National Natural Science Foundation of China (Grants No. 51971112 and 51225102), Jiangsu Province Leading Edge Technology Basic Research Major Project (Grant No. BK20222014) and the Fundamental Research Funds for the Central Universities (Grant No. 30919011405). Q.Z. Mao acknowledges financial supports from the Natural Science Foundation of Jiangsu Province (Grant No. BK20241494). The authors also want to acknowledge the support of the Jiangsu Key Laboratory of Advanced Micro-Nano Materials and Technology. SEM, TEM and EBSD experiments are performed at the Materials Characterization and Research Center of Nanjing University of Science and Technology.

Data availability

Data will be made available on request.

References

[1] S. Zhou, Z. Liu, Z. Lu, L. Ma, Carbon dot/nickel nanocomposite coating for wear and corrosion control of Mg alloy: experimental and theoretical studies, Appl. Surf. Sci. 659 (2024) 159845, https://doi.org/10.1016/j.apsusc.2024.159845.
[2] W. Guo, Q. Bai, K. Deng, Y. Dou, T. Wang, H. Wang, Comparison of lubrication mechanism and friction behavior of graphene on stainless steel substrate at different scales, Appl. Surf. Sci. 649 (2024) 159192, https://doi.org/10.1016/j.apsusc.2023.159192.
[3] G. Zhang, J. Liu, Y. Zhu, T. Shen, D. Yang, Enhanced antibacterial efficacies, corrosion resistance, and cytocompatibility of ZnO/CuO composite coatings through designed sputtering orders, Appl. Surf. Sci. 635 (2023) 157724, https://doi.org/10.1016/j.apsusc.2023.157724.
[4] Y. Wang, S. Li, Z. Zhang, Q. Wang, Z. Song, Q. Zhang, Low-cycle fatigue behavior of zirconium fuel cladding with Cr coatings deposited by high-power impulse magnetron sputtering, Mater. Lett. 353 (2023) 135269, https://doi.org/10.1016/j.matlet.2023.135269.
[5] M. Hu, Y. Tang, X. Han, C. Guo, X. Lu, M. Pan, Failure behavior of Cr coating on PCrNi3MoVA steel under thermal-mechanical factors, Mater. Chem. Phys. 312 (2024) 128691, https://doi.org/10.1016/j.matchemphys.2023.128691.
[6] L. Wang, Q. Liao, J. Zhang, S. Liu, S. Gan, R. Wang, F. Ge, L. Chen, S. Xu, T. Polcar, N. Daghbouj, B. Li, Corrosion behavior of Cr coating on ferritic/martensitic steels in liquid lead-bismuth eutectic at 600 °C and 700 °C, J. Mater. Res. Technol. 29 (2024) 3958–3966, https://doi.org/10.1016/j.jmrt.2024.02.116.
[7] Y. Meng, Y. Sun, M. Li, L. Qi, X. Zhou, H. Shen, S. Zeng, C. Zhu, K. Zhang, C. Chen, X. Han, Improvement of Cr coatings by Mo alloying and the effect of Mo content on the oxidation resistance of CrMo coatings, Surf. Coat. Technol. 478 (2024) 130428, https://doi.org/10.1016/j.surfcoat.2024.130428.
[8] H. Ma, R. Liu, Y. Cui, P. Ke, F. Wang, L. Liu, The effect law of different hydrostatic pressures on the failure of multilayer Cr/GLC coatings in 3.5 wt% NaCl solution, Corros. Sci. 217 (2023) 111120, https://doi.org/10.1016/j.corsci.2023.111120.
[9] T. Zhang, H. Liao, W. Huang, H. Ruan, Y. Su, X. Yang, Z. Xu, S. Yin, J. Wang, High temperature steam oxidation behavior of textured Cr coatings with different grain structures, Surf. Coat. Technol. 459 (2023) 129358, https://doi.org/10.1016/j.surfcoat.2023.129358.
[10] Y. Meng, S. Zeng, C. Chen, C. Zhu, H. Shen, X. Zhou, X. Han, Effect of deposition parameters on characteristics and oxidation behavior of magnetron sputtered Cr coatings, J. Nucl. Mater. 588 (2024) 154802, https://doi.org/10.1016/j.jnucmat.2023.154802.
[11] A.P. Rubshtein, K. Gao, A.B. Vladimirov, S.A. Plotnikov, B. Zhang, J. Zhang, Structure, wear and corrosion behaviours of Cr–Al–C and multilayer [Cr–Al–C/a-C]n coatings fabricated by physical vapour deposition and plasma-assisted chemical vapour deposition techniques, Surf. Coat. Technol. 377 (2019) 124912, https://doi.org/10.1016/j.surfcoat.2019.124912.
[12] E. Tey, Z. Zainal, K.P. Lim, I. Ismail, Influence of nanoparticles concentrations on Cr–C–Al2O3 and Cr–C–SiC nanocomposite coatings electrodeposited from trivalent chromium bath, Mater. Chem. Phys. 310 (2023) 128415, https://doi.org/10.1016/j.matchemphys.2023.128415.
[13] M. Rezaei-Sameti, S. Nadali, J. Rajabi, M. Rakhshi, The effects of pulse electrodeposition parameters on morphology, hardness and wear behavior of nanostructure Cr–WC composite coatings, J. Mol. Struct. 1020 (2012) 23–27, https://doi.org/10.1016/j.molstruc.2012.03.069.
[14] Y. Bian, L. Cao, D. Zeng, J. Cui, W. Li, Z. Yu, P. Zhang, The tribological properties of two-phase hard and soft composite wear-resistant coatings on titanium alloys, Surf. Coat. Technol. 456 (2023) 129256, https://doi.org/10.1016/j.surfcoat.2023.129256.
[15] G. Wolf, E. Halwax, H. Kronberger, Effect of current density and temperature on the morphology of electrodeposited chromium, Met. Finish. 108 (2010) 19–27, https://doi.org/10.1016/S0026-0576(10)80002-9.
[16] M. Assoul, S. Wery, M. De Petris-Wery, G. Gaignier, J. Marti, Relationship between tribological properties of hard chromium coatings and performances of chromium plating electrolyte, Trans. IMF 85 (2007) 135–140, https://doi.org/10.1179/174591907X192258.
[17] J. Yang, P. Ji, J. Zhang, W. Xu, J. Jiao, Y. Lian, L. Jiang, B. Zhang, Effect of current density on the texture, residual stress, microhardness and corrosion resistance of electrodeposited chromium coating, Surf. Coat. Technol. 471 (2023) 129868, https://doi.org/10.1016/j.surfcoat.2023.129868.
[18] B. Podgornik, O. Massler, F. Kafexhiu, M. Sedlacek, Crack density and tribological performance of hard-chrome coatings, Tribology International 121 (2018) 333–340, https://doi.org/10.1016/j.triboint.2018.01.055.
[19] X. Lei, N. Lin, S. Yuan, C. Lei, M. Nouri, Z. Liu, Y. Yu, Q. Zeng, G. Ma, D. Li, Y. Wu, Combining laser surface texturing and double glow plasma surface chromizing to improve tribological performance of Ti6Al4V alloy, Surf. Coat. Technol. 478 (2024) 130418, https://doi.org/10.1016/j.surfcoat.2024.130418.
[20] V.P. Nguyen, T.N. Dang, C.C. Le, Effect of residual stress and microcracks in chrome plating layer to fatigue strength of axle-shaped machine parts, AMM 889 (2019) 10–16, https://doi.org/10.4028/www.scientific.net/AMM.889.10.
[21] G. Bolelli, V. Cannillo, L. Lusvarghi, S. Riccò, Mechanical and tribological properties of electrolytic hard chrome and HVOF-sprayed coatings, Surf. Coat. Technol. 200 (2006) 2995–3009, https://doi.org/10.1016/j.surfcoat.2005.04.057.
[22] M.M. Al-Asadi, H.A. Al-Tameemi, A review of tribological properties and deposition methods for selected hard protective coatings, Tribol. Int. 176 (2022) 107919, https://doi.org/10.1016/j.triboint.2022.107919.
[23] L. Hallez, M. De Petris-Wery, M. Assoul, M. Feki, H.F. Ayedi, Multicriteria optimization of mechanical and morphological properties of chromium electrodeposits under reverse pulse plating, J. Appl. Electrochem. 37 (2007) 843–852, https://doi.org/10.1007/s10800-007-9320-6.
[24] Y. Choi, N.I. Baik, S.I. Hong, Microstructural observation and wear properties of thin chrome layers prepared by pulse plating, Thin Solid Films 397 (2001) 24–29, https://doi.org/10.1016/S0040-6090(01)01352-9.
[25] N. Imaz, E. Garcia-Lecina, J.A. Diez, M. Ostra, M. Sarret, Chemometrics applied to functional chromium electroplating by pulse plating techniques, Trans. Inst. Metal Finish. 90 (2012) 259–266, https://doi.org/10.1179/0020296712Z.00000000046.
[26] I. Celik, B. Benli, The effect of WC-12Co and CrC-NiCr hard coatings applied by HVOF method on the microstructure, mechanical, and surface properties of steel, Metall. Res. Technol. 121 (2024) 318, https://doi.org/10.1051/metal/2024034.

[27] S.H. Sarraf, M. Soltanieh, H. Aghajani, Repairing the cracks network of hard chromium electroplated layers using plasma nitriding technique, Vacuum 127 (2016) 1–9, https://doi.org/10.1016/j.vacuum.2016.02.001.
[28] M.R. Saghi Beyragh, Sh. Khameneh Asl, S. Norouzi, A comparative research on corrosion behavior of a standard, crack-free and duplex hard chromium coatings, Surf. Coat. Technol. 205 (2010) 2605–2610, https://doi.org/10.1016/j.surfcoat.2010.10.009.
[29] J.D.B. De Mello, J.L. Gonçalves, H.L. Costa, Influence of surface texturing and hard chromium coating on the wear of steels used in cold rolling mill rolls, Wear 302 (2013) 1295–1309, https://doi.org/10.1016/j.wear.2013.02.006.
[30] A. Günen, E. Kanca, M.S. Karakaş, M.S. Gök, M. Kalkandelen, B. Kurt, M. Çetin, I. H. Karahan, Effect of thermal degradation on the properties and wear behavior of Cr−V−C composite coatings grown on ductile iron, Surf. Coat. Technol. 419 (2021) 127305, https://doi.org/10.1016/j.surfcoat.2021.127305.
[31] X. Wu, P. Jiang, L. Chen, F. Yuan, Y.T. Zhu, Extraordinary strain hardening by gradient structure, Proc. Natl. Acad. Sci. U. S. A. 111 (20) (2014) 7197–7201, https://doi.org/10.1073/pnas.1324069111.
[32] A. Almotairi, A. Warkentin, Z. Farhat, Mechanical damage of hard chromium coatings on 416 stainless steel, Eng. Fail. Anal. 66 (2016) 130–140, https://doi.org/10.1016/j.engfailanal.2016.04.011.
[33] S. Dal, Y. Altınay, G.A. Çelik, O. Gokcekaya, Ş.H. Atapek, A. Günen, Effect of pack composition on the characteristic and Wear behaviors of Fe-Al Intermetallics grown on AISI 304 stainless steel, J. of Materi Eng and Perform (2025), https://doi.org/10.1007/s11665-025-10695-8.
[34] Protsenko, V.O. Gordiienko, F.I. Danilov, S.C. Kwon, Thick chromium electrodeposition from trivalent chromium bath containing carbamide and formic acid, Metal Finishing 109 (2011) 33–37, https://doi.org/10.1016/S0026-0576(11)80066-8.
[35] Z. Liu, Q. Zhang, X. Zhang, Z. Yu, X. Zhang, Q. Mao, J. Nie, Y. Zhao, Electrodeposition of nanocrystalline Ni and NiCr alloy coatings: effects of Cr content on microhardness and wear resistance improvement, J. Mater. Res. Technol. 30 (2024) 3584–3593, https://doi.org/10.1016/j.jmrt.2024.04.100.
[36] Q. Mao, Y. Liu, Y. Zhao, A review on copper alloys with high strength and high electrical conductivity, J. Alloys Compd. 990 (2024) 174456, https://doi.org/10.1016/j.jallcom.2024.174456.
[37] S.C. Pun, W. Wang, A. Khalajhedayati, J.D. Schuler, J.R. Trelewicz, T.J. Rupert, Nanocrystalline Al-mg with extreme strength due to grain boundary doping, Mater. Sci. Eng. A 696 (2017) 400–406, https://doi.org/10.1016/j.msea.2017.04.095.
[38] Y. Lan, M. Jia, Multiple strengthening mechanisms of grain/twin boundaries, dislocations and nanoprecipitates in mg alloys induced by laser shock processing, Materials Today Communications 38 (2024) 107645, https://doi.org/10.1016/j.mtcomm.2023.107645.
[39] J.H. Seo, S.W. Yoon, K.H. Chae, J.K. Park, J.H. Song, V. Jayaram, K.B. Lee, T. Y. Seong, H. Kwon, J.-P. Ahn, Hardness and nitrogen bonding structure of Al_x Ti_{1-x} N/CrN multilayer hard coating, J. Nanosci. Nanotechnol. 12 (2012) 1581–1584, https://doi.org/10.1166/jnn.2012.4700.
[40] S. Tian, Y. Zhang, A. He, J. Liu, S. Zeng, H. Jiang, Interdiffusion mechanism at the interface between TiAl alloy and NiCoCrAlY bond coating, Surf. Coat. Technol. 444 (2022) 128687, https://doi.org/10.1016/j.surfcoat.2022.128687.
[41] Y. Chen, L. Zhan, Y. Liu, T. Zhou, H. Li, L. Sui, G. Wang, Depositing WC particle coating via SMNAT contributes to a high-quality Ti2AlNb/TA2 joint of diffusion bonding at low temperature, Mater Charact 215 (2024) 114131, https://doi.org/10.1016/j.matchar.2024.114131.
[42] G.M. Erickson, M.A. Sidebottom, J.F. Curry, D.I. Kay, S. Kuhn-Hendricks, M. A. Norell, W.G. Sawyer, B.A. Krick, Paleo-tribology: development of wear measurement techniques and a three-dimensional model revealing how grinding dentitions self-wear to enable functionality, Surf. Topogr.-Metrol. Prop. 4 (2016) 024001, https://doi.org/10.1088/2051-672X/4/2/024001.
[43] J. Joseph, N. Haghdadi, K. Shamlaye, P. Hodgson, M. Barnett, D. Fabijanic, The sliding wear behaviour of CoCrFeMnNi and AlxCoCrFeNi high entropy alloys at elevated temperatures, Wear 428 (2019) 32–44, https://doi.org/10.1016/j.wear.2019.03.002.
[44] Z.Y. Ren, Y.L. Hu, Y. Tong, Z.H. Cai, J. Liu, H.D. Wang, J.Z. Liao, S. Xu, L.K. Li, Wear-resistant NbMoTaWTi high entropy alloy coating prepared by laser cladding on TC4 titanium alloy, Tribol. Int. 182 (2023) 108366, https://doi.org/10.1016/j.triboint.2023.108366.
[45] V. Renciukova, J. Macak, P. Sajdl, R. Novotny, A. Krausova, Corrosion of zirconium alloys demonstrated by using impedance spectroscopy, J. Nucl. Mater. 510 (2018) 312–321, https://doi.org/10.1016/j.jnucmat.2018.08.005.
[46] N.E. Beliardouh, K. Bouzid, C. Nouveau, B. Tlili, M.J. Walock, Tribological and electrochemical performances of Cr/CrN and Cr/CrN/CrAlN multilayer coatings deposited by RF magnetron sputtering, Tribol. Int. 82 (2015) 443–452, https://doi.org/10.1016/j.triboint.2014.03.018.
[47] B. Song, Y. Hua, C. Zhou, Y. Li, L. Yang, Z. Song, Fabrication and anticorrosion behavior of a bi-phase TaNbHfZr/CoCrNi multilayer coating through magnetron sputtering, Corrosion Sci. 196 (2022) 110020, https://doi.org/10.1016/j.corsci.2021.110020.
[48] T. Koseki, J. Inoue, S. Nambu, Development of multilayer steels for improved combinations of high strength and high ductility, Mater. Trans. 55 (2014) 227–237, https://doi.org/10.2320/matertrans.M2013382.
[49] C.X. Huang, Y.F. Wang, X.L. Ma, S. Yin, H.W. Hoeppel, M. Goeken, X.L. Wu, H. J. Gao, Y.T. Zhu, Interface affected zone for optimal strength and ductility in heterogeneous laminate, Mater. Today 21 (2018) 713–719, https://doi.org/10.1016/j.mattod.2018.03.006.
[50] M. Goeken, H.W. Hoeppel, Tailoring nanostructured, graded, and particle-reinforced Al laminates by accumulative roll bonding, Adv. Mater. 23 (2011) 2663–2668, https://doi.org/10.1002/adma.201100407.
[51] H.J. Gao, Y.G. Huang, Geometrically necessary dislocation and size-dependent plasticity, Scr. Mater. 48 (2003) 113–118, https://doi.org/10.1016/S1359-6462(02)00329-9.
[52] Z. Zeng, X. Li, D. Xu, L. Lu, H. Gao, T. Zhu, Gradient plasticity in gradient nano-grained metals, Extreme Mech. Lett. 8 (2016) 213–219, https://doi.org/10.1016/j.eml.2015.12.005.
[53] Y. Zhu, X. Wu, Perspective on hetero-deformation induced (HDI) hardening and back stress, Mater. Res. Lett. 7 (2019) 393–398, https://doi.org/10.1080/21663831.2019.1616331.
[54] N.A. Fleck, M.F. Ashby, J.W. Hutchinson, The role of geometrically necessary dislocations in giving material strengthening, Scr. Mater. 48 (2003) 179–183, https://doi.org/10.1016/S1359-6462(02)00338-X.
[55] R. Randis, D.B. Darmadi, F. Gapsari, A.A. Sonief, E.D. Akpan, E.E. Ebenso, The potential of nanocomposite-based coatings for corrosion protection of metals: a review, J. Mol. Liq. 390 (2023) 123067, https://doi.org/10.1016/j.molliq.2023.123067.
[56] T. Liu, C. Dong, S. Wu, K. Tang, J. Wang, J. Jia, TiN, TiN gradient and Ti/TiN multi-layer protective coatings on uranium, Surf. Coat. Technol. 201 (2007) 6737–6741, https://doi.org/10.1016/j.surfcoat.2006.09.126.
[57] A.E. Rozen, I.S. Los`, D.B. Kryukov, G.V. Kozlov, A.A. Rozen, New multilayer corrosion resistant materials for nuclear power engineering, AMM 770 (2015) 40–44, https://doi.org/10.4028/www.scientific.net/AMM.770.40.